This article has been accepted for publication in a future issue of this journal, but has not been fully edited. Content may change prior to final publication. Citation information: DOI10.1109/tsg.2023.3297451

Model Reduction for Grid-Forming Hybrid Renewable Energy Microgrid Clusters Based on Multi-Timescale Characterization

Zhuoli Zhao, *Member, IEEE*, Xi Luo, Junhua Wu, Jindian Xie, Shaoqing Gong, Qiang Ni, Chun Sing Lai, *Senior Member, IEEE*, and Loi Lei Lai, *Life Fellow, IEEE*

***Abstract*—Due to the high-order model of photovoltaic and wind power generation systems, it is complicated to accurately establish the detailed state-space model of the multi-source renewable energy microgrid (MG) system. In addition, when the MGs are interconnected into microgrid clusters (MGCs), the difficulties of the control and stability analysis are greatly increased. However, the fast and slow dynamics of power electronic interface-based units may not be sufficiently separated on time-scale, which cannot directly follow the assumptions of the traditional model reduction method. This paper selects a typical grid-forming hybrid renewable energy MGC, where the multi-timescale characteristics of the system considering detailed electromagnetic and electromechanical transient modes are analyzed. An identification method without trial-and-error searching for coupling dynamics is proposed under the non-classical singular perturbation characteristics, which is unreported in previous studies and is different from the traditional power systems. Moreover, the reduced-order model can characterize multi-timescale while guaranteeing computational efficiency, which is able to further perform the key parameter optimization and stability analysis for the larger-scale MGCs. The theoretical analysis and the time-domain simulations verify the feasibility and the accuracy of the reduced-order model.**

***Index Terms*—Microgrid clusters, grid-forming, hybrid renewable energy, multi-timescale, reduced-order, non-classical singular perturbation, coupling dynamics.**

This work was supported in part by the National Natural Science Foundation of China 51907031 and 62273104, in part by the Guangdong Basic and Applied Basic Research Foundation 2022A1515011163, in part by the Science and Technology Program of Guangzhou, China 2023A04J0273. (*Corresponding author: Xi Luo; Loi Lei Lai.*)

Z. Zhao, J. Wu, J. Xie, S. Gong, Q. Ni, and L. L. Lai are with the Department of Electrical Engineering, School of Automation, Guangdong University of Technology, Guangzhou, 510006, China (e-mail: zhuoli.zhao@gdut.edu.cn; jhawu73@163.com; 1446939606@qq.com; shaoqing_gong@163.com; nq666@gdut.edu.cn; l.l.lai@ieee.org).

X. Luo is with the Department of Electrical Engineering, School of Automation, Guangdong University of Technology, Guangzhou, 510006, China and also with the Sustainable Energy and Environment Thrust, The Hong Kong University of Science and Technology (Guangzhou), Guangzhou, 511453, China (e-mail: rossellaw@foxmail.com).

C. S. Lai is with the Department of Electronic and Electrical Engineering, Brunel University London, London, UB8 3PH, UK and also with the Department of Electrical Engineering, School of Automation, Guangdong University of Technology, Guangzhou, 510006, China (e-mail: chunsing.lai@brunel.ac.uk).

I. Introduction

THEORETICALLY, microgrid (MG) and microgrid clusters (MGCs) are not only conducive to the local consumption of renewable energy (RE), but also provide an effective solution for the voltage-source distributed generation mode in the high-penetration RE system [1], [2]. The control and stability analysis of MGs and MGCs based on the state-space model have attracted much attention in recent years [3]-[5]. The state-space model is able to describe the transient performance process of the system and is a general tool for describing the system dynamics [6], [7]. In fact, the difficulties of the system control and stability analysis problem are significantly increased when the MGs are interconnected into MGCs.

Firstly, it is complicated to accurately establish the detailed state-space model of the multi-source RE system. The battery energy storage system (BESS) and the photovoltaic (PV) system model reach more than ten orders and the variable-speed wind turbine model considering multi-mass can reach more than 20 orders [4], [5], [8]. Including the networks, tie-lines and load models of the MG system, the integrated system model can reach hundreds of orders. Secondly, the number of power electronic devices in the system is huge, and the RE units with power electronic interfaces have wide time-scale characteristics ranging from microseconds to seconds. Therefore, the urgent need of small time-step and long-time simulation put forward higher requirements for the digital simulation of the MGCs, and the burden of analysis and calculation increases sharply.

However, the appropriate model reduction can effectively simplify the system's complexity and reduce the computational burden of digital simulation. The classical singular perturbation (SP) theory is effectively applied to model simplification and order reduction, with the principle that the fast and slow dynamics are independent decoupling to a certain extent. Therefore, the state variables of the system can be divided into the fast and slow subsystems [9]. The SP theory has been successfully applied in traditional power systems based on synchronous generator (SG) for many years [10]. In [11] and [12], the traditional power system considers ignoring the fast electromagnetic transients in the electromechanical transient analysis of the SG, which the low-order simplified model of SG such as third-order and second-order model can be obtained. In the view of [13], the reduced-order mathematical basis of the traditional power system is that the SG dominated-power

Copyright © 2023 Institute of Electrical and Electronics Engineers (IEEE). Personal use of this material is permitted. Permission from IEEE must be obtained for all other uses, in any current or future media, including reprinting/republishing this material for advertising or promotional purposes, creating new collective works, for resale or redistribution to servers or lists, or reuse of any copyrighted component of this work in other works by sending a request to pubs-permissions@ieee.org. For more information, see https://www.ieee.org/publications/rights/rights-policies.html

This article has been accepted for publication in a future issue of this journal, but has not been fully edited. Content may change prior to final publication. Citation information: DOI10.1109/tsg.2023.3297451

system has excellent SP characteristics, which can be regarded as the dual time-scale system. It is reflected in the significant difference as well as relatively independent between the time-scale of slow dynamics and fast dynamics, which is less interactive coupling [14].

In recent years, many studies have attempted to use SP method directly to the model reduction of grid-tie inverter or islanded inverter system, trying to describe the inverter-interface units in power system. The model reduction of grid-tied and islanded MG models is respectively carried out in [15]. Using the SP method, the low-order model improves the computation efficiency and recovers the original system response under dual time-scale analysis. In [16], the SP method is also adopted for model reduction of the islanded MG, while the coupling capacitors of the *LCL* filters are ignored in the modeling. This simplification has unacceptable modeling errors, especially when the inverter is used for the voltage and frequency regulation in autonomous system. The reduction of multi-inverters MG using grid-forming strategy is carried out in [17], which simply eliminated the fast dynamics such as network and coupling inductance step by step. It is further found that not all the inverters have the same contribution to the small-signal stability of MG. Therefore, the identification method of critical clusters in the system is proposed, which is helpful in obtaining accurate low-order models. Multiple reduced-order model comparisons of the inverter interfaced unit with droop control are examined in [18] and the Lyapunov stability analysis is given in [19]. They prove the accuracy as well as stability of system performance of the multiple low-order model. Besides, some researches are also reported to conduct the stability analysis of reduced-order models. [20] directly uses the existing SP technique to ignore the internal fast dynamics for dynamic stability analysis of the reduced-order model. Moreover, [21] further investigates the convergence behavior of singularly perturbed inverter-based MG. And the effects of modeling uncertainty and different loading conditions on the effectiveness of the reduced-order model are also discussed.

There are also other works that report to conduct the MG model reduction using other than SP method. The approximate Kron reduction for networks is presented in [22]. And the order reduction method that can identify significant lines and interaction modes is proposed in [23] for stability perspective. But they only focus on the electrical networks without considering the dynamics of the units. The aggregate model is proposed in [24] and the dynamic equivalent modeling method is presented for the MGC in [25]. The equivalence is to aggregate inverters with the same control loops. However, the interactions among different units cannot be explored. The dynamic phasors-based reduced-order model in [26] is applied for the inverter-based MG to predict the trend of the eigenvalue movement and the stability margins. Moreover, [27] uses balanced transformation, SP and pole clustering methods to compare the dynamic characteristics of the virtual synchronous generator and the droop-control inverters.

In the study of the MGs or MGCs model reduction, it is essential to accurately characterize the system dynamics. In [15]-[21], the classical dual time-scale method is used to establish various inverter-based reduced-order models. However, the fast and slow dynamics of RE units based on the power electronic interface may not be sufficiently separated on time-scale. It presents the characteristics of coupling dynamics, even the coupling interaction between the fast and slow dynamics, which will lead to the significant difference of the time-scale characteristics between the RE-MGCs and the traditional power system. Therefore, the direct elimination of fast dynamics may lead to the disappearance of some system dynamics and significantly affect the modeling accuracy. [28] demonstrates that in the system with insufficient time-scale separation, some fast dynamics with small participation factors but interacting with slow dynamics cannot be discarded. The participation of these fast states needs to be restored in the slow sub-model. However, the research in [28] does not explicitly illustrate the characteristics of the coupling dynamics. Moreover, there is no identification method of coupling dynamics. Therefore, how to identify and even quantify the characteristics of the coupling interactions under the non-classical SP characteristics has become the critical issue of model reduction for power-electronized power systems.

Furthermore, the current researches on order reduction of MGs or MGCs in [15]-[28] are only limited to systems based on ideal BESS units, rather than the actual primary energy modeling of RE units like PV and wind turbine. In fact, in our previous studies, the DC-link dynamics of PV array are considered in [5] and the oscillations caused by the changes of DC-link dynamics are studied in [29]. Besides, the rotor speed dynamics of wind turbine are considered in [30]. They both illustrate that ignoring the dynamics of the primary sources and assuming them as constant DC voltages for simplicity in stability investigations of MGCs may lead to misleading analytical results. Therefore, the modeling of primary energy is essential to accurately describe the dynamic characteristics of the RE-MGCs and to guarantee the accuracy of the reduced-order model.

Therefore, with the detailed primary energy sources modeling of the RE generation units, the influence of the coupling interactions between the fast and slow dynamics on the MG/MGCs model reduction is still a research gap. In current literature [15]-[21], only using the dual time-scale classical SP method may affect the modeling accuracy; only simplifying to constant DC voltage may mislead the analytical results in [15]-[28].

Motivated by the aforementioned research gap, this paper uses non-classical SP characteristics and considers the addition of coupling dynamics to achieve the accurate system order reduction of the multi-source hybrid RE-MGC. The main contributions of this paper are summarized as follows:

1) The primary energy dynamics are the critical element of the full-order model. Different from traditional model reduction studies that ignore primary energy dynamics, in this paper, the multi-timescale characteristics of the grid-forming hybrid RE-MGC system considering detailed electromagnetic and electromechanical transient modes are analyzed.

2) Due to the unpredictable characteristic of coupling

This article has been accepted for publication in a future issue of this journal, but has not been fully edited. Content may change prior to final publication. Citation information: DOI10.1109/tsg.2023.3297451

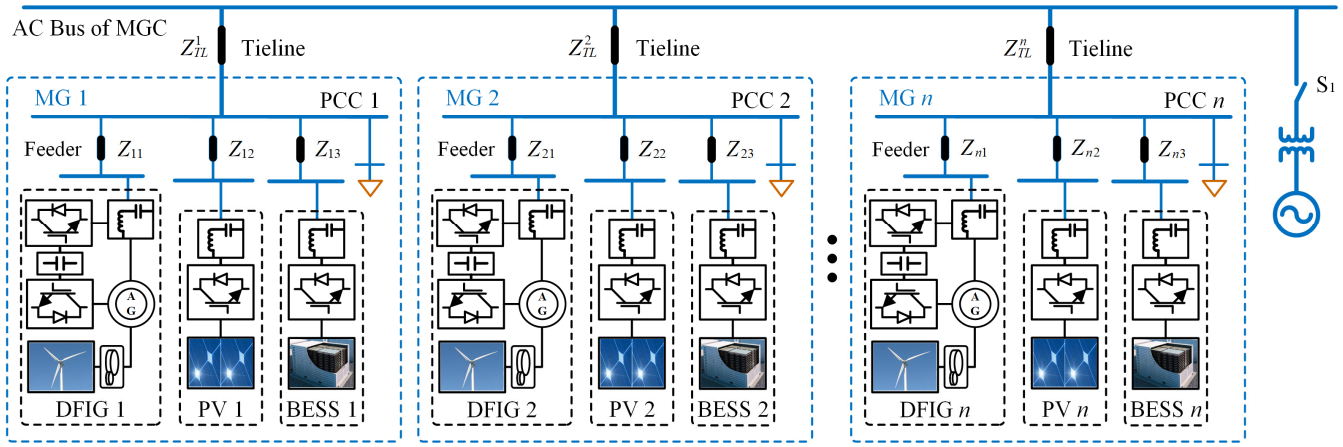

Fig. 1. Topology architecture of the hybrid renewable energy microgrid clusters.

dynamics hidden in fast and slow dynamics, all the dynamics that strongly associated to the dominant modes are only unconditionally reserved in the traditional method, simply considering them to be slow dynamics without identifying the coupling dynamics. A classification criterion of system dynamics and an identification method without trial-and-error searching for coupling dynamics are proposed under the system characteristics of non-classical singular perturbation, which is unreported in previous studies and is different from the traditional power systems.

3) Based on the non-classical singular perturbation characteristics, the model reduction of the typical grid-forming hybrid RE-MGC is conducted. The reduced-order model reserves the coupling dynamics as well as the global slow dominant dynamics, which can characterize multi-timescale while guaranteeing computational efficiency.

This paper is organized as follows. Section II presents the multi-timescale identification analysis under the modeling of the studied MGC. Section III elaborates the non-classical SP characteristics and proposes the identification method of coupling dynamics as well as the generalized model reduction method. Section IV proposes the model reduction of multi-source MGC and obtains a reduced-order model. Section V presents the time-domain simulation results of the model response. Finally, the conclusion is given in Section VI.

II. Modeling and Multi-Timescale Analysis of Hybrid Renewable Energy Microgrid Clusters

Under the consideration of the increasing penetration of hybrid RE integrated into the distribution network, Fig. 1 shows the topology architecture of the studied hybrid renewable energy MGC. This autonomous MGC architecture can be specifically applied to the advanced distribution network operation or some remote area which is rich in solar energy and wind energy [5], [30]. In this scenario, power supply can be available for production, living, tourism, etc. In a single MG in Fig. 1, a DFIG unit, a PV unit and a supplementary BESS unit are implemented via resistive-inductive feeders for power supply to local loads. In the case of high-penetration RE operation, each unit of the system operates in a grid-forming strategy, which is also the islanded operation mode studied in this work. In this section, a unit-to-system modeling approach is adopted.

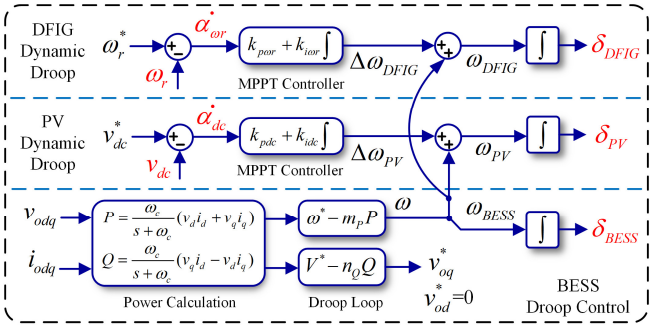

Fig. 2. Grid-forming droop loop of DFIG, PV and BESS model.

A. Modeling of Grid-Forming Hybrid Renewable Energy Units

In our previous research, we have proposed grid-forming control strategies for PV and wind power generations under weak grid conditions [5], [29], [30]. The grid-forming strategy enables RE units not to rely on precise phase-locking of strong power grids, most importantly, the RE units can participate in system frequency regulation and voltage support under weak grid conditions.

As the widely used commercial wind power generator, DFIG has the advantage of small-capacity and low-cost power converters. It has the special structure that the stator of the asynchronous generator (AG) is connected to the MG bus, and the back-to-back (B2B) converters only transmit the slip power. Firstly, the wind turbine is connected to the AG via the speed-increasing gear. The state-space model of the wheel-gear-rotor drive train shaft model and the AG can be given by:

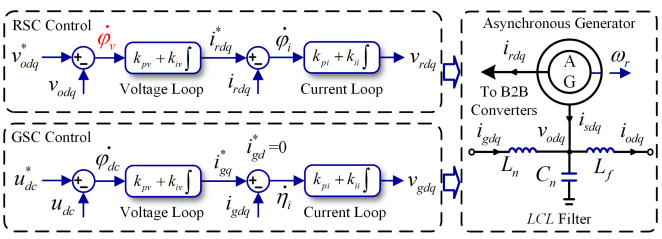

Fig. 3. B2B converters control loops, AG and *LCL* filter of DFIG model.

This article has been accepted for publication in a future issue of this journal, but has not been fully edited. Content may change prior to final publication. Citation information: DOI10.1109/tsg.2023.3297451

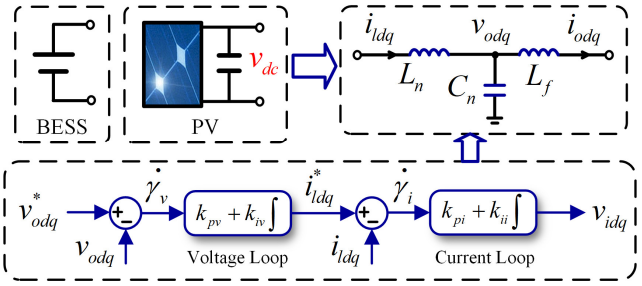

Fig. 4. Converters control loops and *LCL* filter of PV and BESS model.

TABLE I
SYSTEM PARAMETERS OF MICROGRID CLUSTERS

Parameter	Symbol	Value
Electrical parameters		
Tie-line and feeder	$Z_{TL}^{1/2/3}, Z_{11\sim33}$	0.575 + *j*0.25 (Ω), 0.115 + *j*0.05 (Ω)
LCL filter	$L_n^{DFIG}, L_n^{PV/BESS}, C_n^{DFIG}, C_n^{PV/BESS}, L_f^{DFIG}, L_f^{PV/BESS}$	4mH, 1.35mH, 50μF, 50μF, 1mH, 0.75mH
Control parameters		
MPPT loop	$k_{p\omega r}, k_{i\omega r}, k_{pdc}, k_{idc}$	$3e^{-3}$, $4e^{-3}$, $8e^{-4}$, $3e^{-3}$
Droop loop	$m_p^{DFIG/PV/BESS}, \omega^*, n_Q^{DFIG/PV/BESS}, V^*$	$5.027e^{-5}$, 100π rad/s, $1.267e^{-4}$, 380V
Voltage loop	$k_{pv}^{DFIG\cdot RSC}, k_{iv}^{DFIG\cdot RSC}, k_{pv}^{DFIG\cdot GSC}, k_{iv}^{DFIG\cdot GSC}, k_{pv}^{PV/BESS}, k_{iv}^{PV/BESS}$	0.1, 25, 0.3, 6, 0.05, 390
Current loop	$k_{pi}^{DFIG\cdot RSC}, k_{ii}^{DFIG\cdot RSC}, k_{pi}^{DFIG\cdot GSC}, k_{ii}^{DFIG\cdot GSC}, k_{pi}^{PV/BESS}, k_{ii}^{PV/BESS}$	10, 500, 25, 23, 10.5, $16e^3$

$$\Delta\dot{x}_{SM} = A_{SM}\Delta x_{SM} + B_{SM1}\Delta i_{sdq} + B_{SM2}\Delta i_{rdq} \quad (1)$$

$$\Delta\dot{x}_{AG} = A_{AG}\Delta x_{AG} + B_{AG1}\Delta v_{rdq} + B_{AG2}\Delta v^*_{odq} + B_{AG3}\Delta\omega_r \quad (2)$$

In (1)-(2), $\Delta x_{SM} = [\Delta\omega_{wheel}\ \Delta T_m\ \Delta\omega_r]^T$; $\Delta x_{AG} = [\Delta i_{sdq}\ \Delta i_{rdq}]^T$. $\Delta\omega_{wheel}$, ΔT_m and $\Delta\omega_r$ are the state variables of wind wheel speed, output mechanical torque and rotor speed, respectively. Δi_{sdq}, Δi_{rdq} and Δv_{rdq} are the state variables of stator currents, rotor currents and rotor voltages of the AG, respectively. Note that A_{SM}, B_{SM}, A_{AG} and B_{AG} can be found in the Appendix, which are derived from the ordinary differential equations (ODEs) in [30] representing the shaft model and AG of DFIG. Besides, the parameters of the AG are the same as [30].

Secondly, the grid-forming strategy is based on the dynamic droop loop, as shown in Fig. 2. The droop loop can provide the power angle and voltage reference for each unit in order to make them capable of participating in frequency regulation and voltage control in autonomous mode. The three units share the same droop loop, but the DFIG and PV have a supplemental maximum power point tracking (MPPT) controller attached to the droop loop, as presented in [5], [29], [30]. The control loop of the B2B converters (rotor-side converter (RSC) and grid-side converter (GSC)) and its controlled objects (i.e., AG and *LCL* filter) are shown in Fig. 3. In conclusion, the state-space model of the grid-forming DFIG in synchronous reference frame can be given as follows:

$$\Delta\dot{x}_{DFIGi} = A_{DFIG}\Delta x_{DFIGi} + B_{DFIG}\Delta v_{bDQi} + B_{comi}\Delta\omega_{com} \quad (3)$$

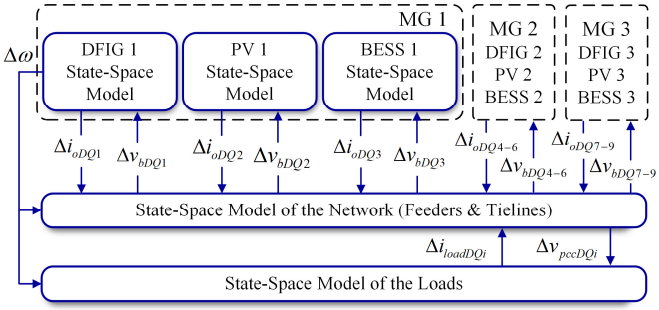

Fig. 5. Modeling framework of MGC.

$$\Delta x_{DFIGi} = \left[\Delta x_{Droop}^{DFIG}\ \Delta x_{SM}\ \Delta x_{AG}\ \Delta x_{LCL}^{DFIG}\ \Delta x_{RSC}\ \Delta x_{GSC}\right]^T \quad (4)$$

where Δx_{DFIG} are the state variables of each component and $\Delta x_{Droop}^{DFIG} = [\Delta\alpha_{\omega r}\ \Delta\delta_{DFIG}\ \Delta P_{DFIG}\ \Delta Q_{DFIG}]^T$. Δv_{bDQ} are the connection point voltages in the synchronous reference frame of DFIG system and $\Delta\omega_{com}$ is an additional input signal of the frequency deviation between the local and synchronous reference frame. A_{DFIG} is the system matrix that combines all the components and control loops of the DFIG. And A_{DFIG}, B_{DFIG} also can be derived from the ODEs in [30].

PV and BESS share a similar voltage and current control loop and circuit configuration, as shown in Fig. 4. Besides, the DC link voltage dynamic of the PV is under consideration in Fig. 2, which is a supplemental MPPT controller like DFIG. Therefore, the state-space model of the grid-forming PV and BESS in the synchronous reference frame are developed in (5)-(8):

$$\Delta\dot{x}_{PVi} = A_{PV}\Delta x_{PVi} + B_{PV}\Delta v_{bDQi} + B_{comi}\Delta\omega_{com} \quad (5)$$

$$\Delta x_{PVi} = [\Delta x_{Droop}^{PV}\ \Delta v_{dc}\ \Delta x_{LCL}^{PV}\ \Delta\gamma_{vdq}\ \Delta\gamma_{idq}]^T \quad (6)$$

$$\Delta\dot{x}_{BESSi} = A_{BESS}\Delta x_{BESSi} + B_{BESS}\Delta v_{bDQi} + B_{comi}\Delta\omega_{com} \quad (7)$$

$$\Delta x_{BESSi} = [\Delta x_{Droop}^{BESS}\ \Delta x_{LCL}^{BESS}\ \Delta\gamma_{vdq}\ \Delta\gamma_{idq}]^T \quad (8)$$

In (6) and (8), $\Delta x_{Droop}^{PV} = [\Delta\alpha_{dc}\ \Delta\delta_{PV}\ \Delta P_{PV}\ \Delta Q_{PV}]^T$ and $\Delta x_{Droop}^{BESS} = [\Delta\delta_{BESS}\ \Delta P_{BESS}\ \Delta Q_{BESS}]^T$. Note that A_{BESS}, B_{BESS} and B_{comi} are given in detail in [31]. A_{PV} and B_{PV} are the same structure with BESS and can be derived in [5] and the parameters of PV array are also identical to [5]. In addition, the other parameters of the MGC are given in Table I.

B. The Full-Order Dynamic Model of Microgrid Clusters

According to the unit-to-system modeling method, the state-space model of the network (i.e., feeders and tie-lines) and the load are established respectively, then the MGC modeling is realized according to the framework in Fig. 5. Now, combined with all the distributed generation units, network, loads, the integrated dynamic model of MGC in Fig. 1 can be and readily constructed as:

$$\Delta\dot{x}_{MGC} = A_{MGC}\Delta x_{MGC} \quad (9)$$

$$\Delta x_{MGC} = [\underbrace{\Delta x_{BESS1}\ \Delta x_{PV1}\ \Delta x_{DFIG1}\ \Delta x_{line}\ \Delta x_{load}}_{\Delta x_{MG1}}\ \underbrace{\cdots}_{\Delta x_{MGj}}\ \Delta x_{tie}]^T \quad (10)$$

This article has been accepted for publication in a future issue of this journal, but has not been fully edited. Content may change prior to final publication. Citation information: DOI10.1109/tsg.2023.3297451

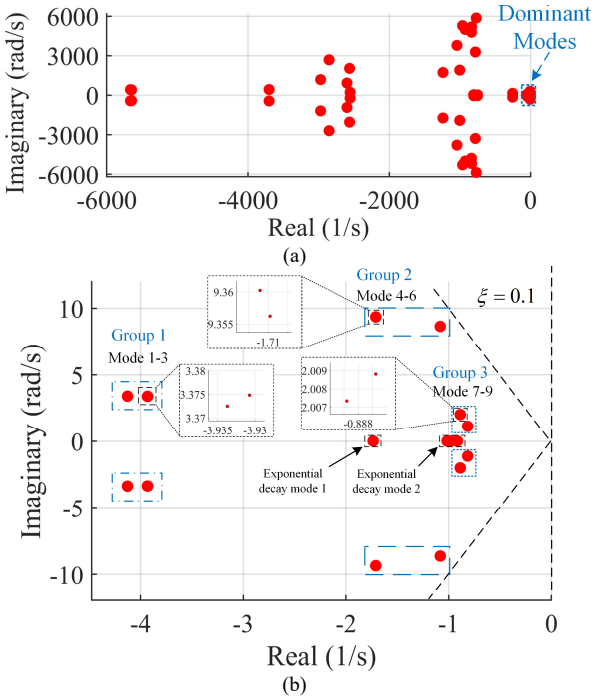

Fig. 6 (a). Overview modes of MGC. (b) Dominant modes of MGC.

Based on the established small-signal model, the overview modes and dominant modes of the MGC can be obtained with a certain typical steady-state operating point, as shown in Fig. 6. The nine pairs of complex-conjugate eigenvalues are divided into three oscillation groups while the other negative real eigenvalues are divided into two exponential decay (ED) groups. In Fig. 6 (b), all the oscillation modes have the damping ratios (ξ) greater than 0.1 as recommended in [32], [33].

C. *Analysis of System Multi-Timescale*

The coexistence of dynamic processes in different time-scale is a universal physical phenomenon. Fig. 7 shows the schematic diagram of the multi-timescale dynamic characteristics of the MGC system. Different from the traditional MG analysis in [28], [31], the hybrid RE unit considering the solar/wind primary energy will introduce the electromagnetic transient and electromechanical transient modes in the slower time-scale dynamics. On the other hand, the system includes resistive-inductive networks, power electronic devices, mechanical components, etc., and has wide time-scale characteristics ranging from microseconds to milliseconds to seconds. The multi-timescale characteristics of the system are analyzed in this part.

1) *Dominant Slow Dynamics*

The derived dynamic model in (9) is then adopted to evaluate the small-signal stability of the MGC, which is shown in Fig. 6. The dimension of x_{MGC} described by state matrix A_{MGC} is 189. Except for the dominant oscillation modes of the system corresponding to the dominant eigenvalues, the remaining modes can be identified as high-frequency and high-damping oscillation modes with higher decay speeds. Therefore, only the low-frequency modes are identified as the dominant oscillation modes, which dominate the system performance and are the main focus of this study. The dominant modes are selected in Fig. 6 (b). To identify the correlation between system states and dominant modes, the participation factor (PF) analysis is carried out in Table II. In addition, the calculation method of the PF is detailed in [14], [31].

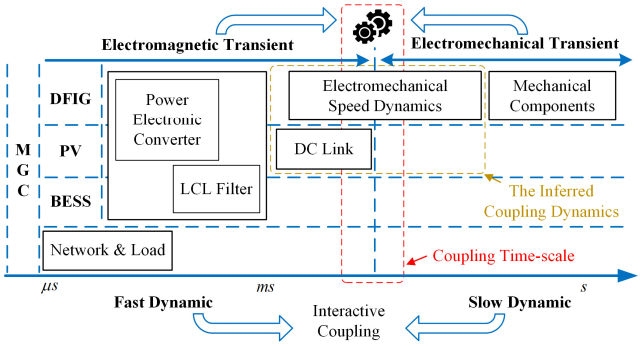

Fig. 7. Multi-timescale dynamic characteristics of the MGC system.

TABLE II
RESULTS OF PARTICIPATION FACTOR ANALYSIS OF DOMINANT MODES

Modes	Strongly associated units	Strongly associated states
Group 1 Mode 1-3	PVs and DFIGs	$\Delta\delta$, ΔP , $\Delta\alpha_{dc}$, Δv_{dc} , $\Delta\omega_r$, $\Delta\omega_{wheel}$, ΔT_m, $\Delta\varphi_{vdq}$
Group 2 Mode 4-6	DFIGs and PVs	$\Delta\delta$, ΔP , Δv_{dc} , $\Delta\omega_r$, $\Delta\omega_{wheel}$, ΔT_m
Group 3 Mode 7-9	DFIGs	$\Delta\delta_{DFIG}$, $\Delta\alpha_{or}$, $\Delta\omega_r$, $\Delta\omega_{wheel}$, ΔT_m
Exponential decay mode 1	DFIGs	$\Delta\delta_{DFIG}$, $\Delta\alpha_{or}$, $\Delta\omega_r$, $\Delta\omega_{wheel}$
Exponential decay mode 2	DFIGs	$\Delta\omega_r$, $\Delta\omega_{wheel}$, ΔT_m , $\Delta\eta_{idq}$

Furthermore, to study the system characteristics and dominant performance, it is necessary to focus on the complex-conjugate eigenvalues. They affect system performance in the form of damped oscillations while the negative real eigenvalues are not the main focus. Fig. 8 illustrates the normalized state variables PF of the strongly associated states of each damped oscillations mode. The states strongly associated with the dominant modes can greatly affect the dynamic response of the system performance and they can be identified as globally dominant slow dynamics. The dominant slow dynamics mainly include the power controllers, wind and solar MPPT controllers, RSC voltage controllers, DC-link voltage and shaft model, proving that the slow dynamics are mainly affected by PV and DFIG. Moreover, the identified slow dynamics are marked in red font in the modeling diagram (i.e., Fig. 2-Fig. 4).

2) *Coupling Time-Scale*

As seen in Fig. 7, under the action of the control loops and the physical rotor structure, the electromechanical speed dynamics of the DFIG spanned from the electromagnetic transient to the electromechanical transient on time-scale. The characteristic of time-scale coupling reveals that there may be interactive coupling between the fast and slow dynamics. The PF results of Group 1-2 in Fig. 8 illustrate that the outer dynamic droop loops of the PV units, the shaft models and the RSC voltage controllers contribute to these dominant oscillation modes. Table III shows the average participation

This article has been accepted for publication in a future issue of this journal, but has not been fully edited. Content may change prior to final publication. Citation information: DOI10.1109/tsg.2023.3297451

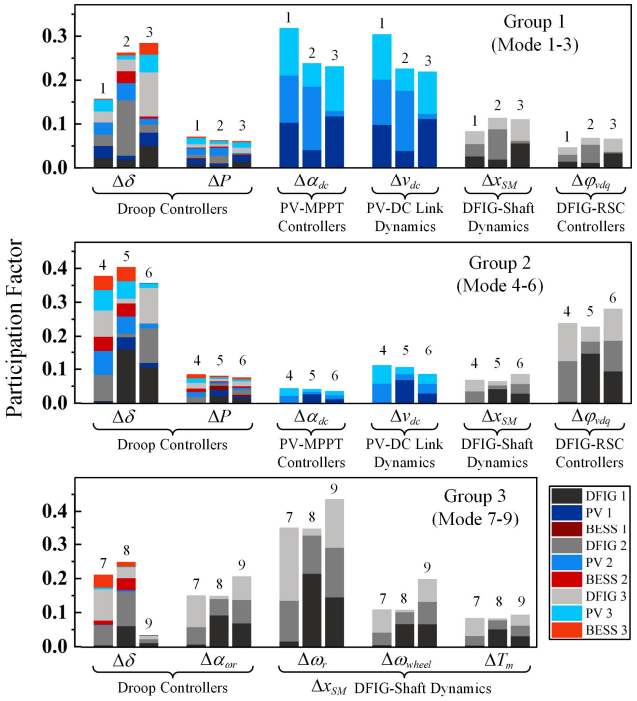

Fig. 8. The normalized participation factors of strongly associated states of each damped oscillations mode.

proportion of parts of DFIG/PV variables contributing to Group 1-2. It is concluded that Mode 1-6 are almost dominated by PVs and DFIGs, in which reasonable coupling of the power angle due to the units' autonomous operation in MGC. Besides, both the DC-link dynamic of the PV and the electromechanical part of the DFIG contribute to the same dominant oscillation mode, revealing that it is possible for the PV and DFIG unit to interact in a nearby time-scale. Moreover, in previous studies, the voltage outer loop is considered as the fast dynamic with fast decay. But in this study, the RSC voltage loops of DFIGs occupy about a quarter of the participation proportion in Group 2 especially. Looking back to Fig. 2 and 3, the RSC voltage controller is between the power controller and the current controller, that is, the middle of the slow dynamic of the outer loop and the fast dynamic of the inner loop, which is reasonable to infer that these states have special time-scale. As shown in Fig. 7, it can be temporarily inferred that both the electromechanical speed dynamics and DC-link have the characteristics of coupling dynamics. Therefore, different units may have interactive coupling, and the coupling time-scale represents the coupling of fast and dominant slow dynamics, further demonstrating the coupling states existing in the system, which is the crucial point in this study.

3) Fast Dynamics

The remaining modes with the high frequency and high damping are mainly strongly associated with the states of currents of feeders, tie-lines and loads. Besides, some fast modes are associated with the PV/BESS current controllers, states variables of the *LCL* filters. These mentioned states have extremely small participation factors of dominant slow modes and they can be ignored in the analysis. Therefore, this sort of states only correlates with the fast modes, obviously identified

TABLE III
AVERAGE PARTICIPATION PROPORTION OF GROUP 1-2

Average Participation Proportion	$\Delta\delta_{PV}$	$\Delta\alpha_{dc}, \Delta v_{dc}$	$\Delta\delta_{DFIG}$	Δx_{SM}	$\Delta\varphi_{vdq}$
Group 1 Mode 1-3	7.44%	51.20%	13.85%	10.24%	6.01%
	PV in total: 62.30%		DFIG in total: 35.04%		
Group 2 Mode 4-6	10.50%	14.10%	22.01%	7.27%	24.89%
	PV in total: 28.20%		DFIG in total: 63.64%		

as fast dynamics in dual time-scale systems, which exhibit extremely fast decay under disturbance compared with the slow dynamics. The fast states have negligible effects on the exact location of the dominant parts and they will be eliminated in the reduced-order model [9], [17]. It should be noted that in this paper, the slow dominant dynamics and the coupling dynamics are the focus of constructing reduced-order model, while fast dynamics contribute less.

III. GENERALIZED MODEL REDUCTION METHOD OF NON-CLASSICAL SINGULAR PERTURBATION SYSTEM

A. Dual Time-Scale Singular Perturbation Theory and Reduced-Order Equivalence

The classical SP theory can be effectively used for model order reduction. The system represented by Equation (9) covers a wide range of time-scale and the theory of classical SP can be applied. Based on the appropriate selection of parameter ε, the original coupling system can be described through various combinations:

$$\begin{cases} \dot{x}_{MGC\text{-}s} = f(x_{MGC\text{-}f}, x_{MGC\text{-}s}, u) \\ \varepsilon \dot{x}_{MGC\text{-}f} = g(x_{MGC\text{-}f}, x_{MGC\text{-}s}, u) \end{cases} \tag{11}$$

where $x_{MGC\text{-}s}, x_{MGC\text{-}f}$ are the dominant slow dynamics and fast dynamics, respectively. u is the input of the system and ε is the SP parameter, which is generally with small values such as stray inductance and capacitance.

$$x_{MGC\text{-}f} = h(x_{MGC\text{-}s}, u) \tag{12}$$

$$\dot{x}_{MGC\text{-}s} = f[x_{MGC\text{-}s}, h(x_{MGC\text{-}s}, u), u] \tag{13}$$

Considering the decoupling of the original dual time-scale system, the fast dynamics can be treated as a boundary layer system by approximating ε to zero in (11) and Equation (12) can be obtained [9]. Therefore, the full-order systems exhibiting dual time-scale can be reduced based on the SP theory in (13).

B. Non-Classical Singular Perturbation Characteristics

In Section III-A, the SP method is used for dual time-scale model reduction. However, model reduction should firstly identify the number of fast and slow dynamics, reserving slow states as state variables, simplifying the other states as intermediate variables and treating as the boundary layer. When applying the classical SP method for model reduction and equivalence, the following judgments should be satisfied:

a) The dominant slow dynamics x_s should be strongly associated with the slow eigenvalues (i.e., dominant slow

This article has been accepted for publication in a future issue of this journal, but has not been fully edited. Content may change prior to final publication. Citation information: DOI10.1109/tsg.2023.3297451

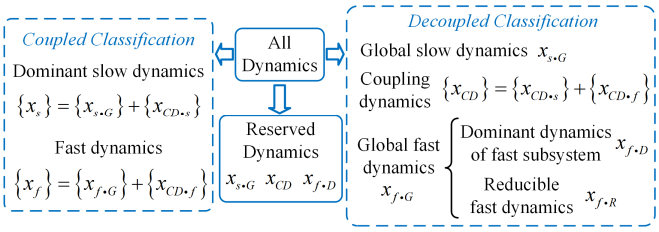

Fig. 9. Classification of the system dynamics.

modes), and the dimension of x_s equals to the number of slow modes. At the same time, the fast dynamic should only relate to the fast eigenvalues and the fast modes.

b) The application of classical SP method cannot basically affect the exact location of the system's slow dominant modes after order reduction. Moreover, after confirming x_s , if x_s are eliminated as the constant value, the fast eigenvalues of the system can be calculated. Then it should be ensured that the calculated fast eigenvalues coincide with the original system.

In conclusion, if the studied system does not strictly satisfy the above conditions, it is considered that the system exhibits non-classical SP characteristics. Therefore, the equivalence and order reduction of the system cannot only rely on the classical SP method because of the dual time-scale insufficient separation.

C. Coupling Dynamics under Non-Classical Singular Perturbation

As discussed above, the studied MGC system has different dynamics in a wide range of time-scales. As the basis of reduced-order modeling in Section III-A, the classical SP theory can be applied in a dual time-scale system for model equivalence.

However, using the above judgments is not enough for model reduction of the power electronic interface-based unit. The fast and slow dynamics of the power electronic interface-based RE units may not be sufficiently separated or even have significant coupling interactions in the nearby time-scale. For example, some coupling dynamics may have both fast and slow dynamic components, and it is not necessarily a classical SP system.

Typically, under non-classical SP characteristics, the number of slow states is not equal to the slow modes, which infers that some coupling dynamics may exhibit. If some of the coupling dynamics get the characteristics of both fast and slow dynamics, the number of slow dynamics will be larger than the slow modes. If the redundant coupling dynamics are ignored, it will affect the accuracy of the reduced-order model though it reflects the properties of the original boundary layer under the classical SP system. If the coupling dynamics are reserved, the accuracy can be ensured, but the remaining dynamics constituting the algebraic constraints are different from the original boundary layer [9], [34], [35]. It is necessary to separate the coupling dynamics from the slow dynamics by establishing the fast subsystem. Firstly, the slow dynamics are determined based on the correlation with the slow modes. Then, supposing the slow dynamics as input nearby the steady-state point, calculate the eigenvalues constraining by the remaining fast dynamics. If the eigenvalues calculated coincide with the original fast modes,

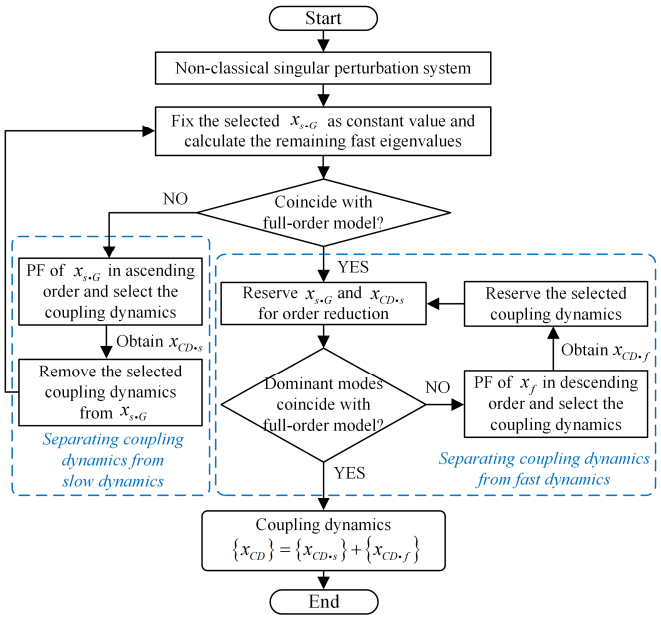

Fig. 10. The flowchart of identification method of coupling dynamics.

the SP characteristics of the original system can be reflected. And the correctness of the selected slow and fast dynamics (without coupling dynamics) can be guaranteed as well.

Furthermore, as a typical inverter-based system, MGC has a significant time-scale characteristics difference compared with traditional power systems. If applying classical SP, the direct elimination of fast dynamics may lead to the disappearance of some system dynamics and significantly affect the modeling accuracy. Therefore, in order to ensure the accuracy, it is particularly important first to identify and then reserve the coupling dynamics in the reduced-order model.

D. Identification Method of Coupling Dynamics

If using the traditional judgment, the numbers of slow/fast dynamics and slow eigenvalues need to be accurately calculated, and the excess parts can be determined as the number of coupling dynamics. However, for systems whose time-scale is not sufficiently separated, the calculations will be difficult. It is necessary to build an accurate and fast identification method without trial-and-error searching for the coupling dynamics.

To more clearly identify the coupling dynamics, the existing dynamics of the system need to be classified and Fig. 9 carries out the classification. In coupled classification, fast/slow dynamics consist of global fast/slow dynamics and coupling dynamics, which can describe the coupling dynamics hidden in fast/slow dynamics or behaving as fast/slow dynamics in other words. In decoupled classification, the coupling dynamics are separated from the fast/slow dynamics and only global fast/slow dynamics are considered. The global fast dynamics $x_{f\cdot G}$ includes reducible fast dynamics $x_{f\cdot R}$ and the dominant dynamic of fast subsystem $x_{f\cdot D}$. Note that while $x_{f\cdot D}$ belong to the fast dynamics according to the PF results, they are constrained by the system modeling framework (seen in Fig. 5), which can dominate fast subsystem and affect the modeling accuracy. For example, Δi_{oDQi} in Fig. 5 represents the unit

This article has been accepted for publication in a future issue of this journal, but has not been fully edited. Content may change prior to final publication. Citation information: DOI10.1109/tsg.2023.3297451

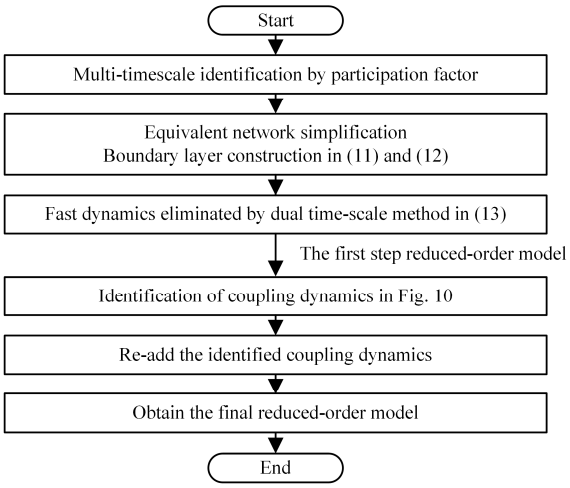

Fig. 11. The proposed generalized model reduction method of non-classical singular perturbation system.

output current in the synchronous reference frame. As a medium between the RE unit and network model, it will lead to the failure of modeling if it is eliminated as the fast dynamics.

Besides, because of the unpredictable characteristic of coupling dynamics hidden in fast/slow dynamics, x_{CD} may come from both fast and slow dynamics. The reducible fast dynamics $x_{f\bullet R}$ can be directly eliminated as boundary layer using the SP method. And the global slow dynamics $x_{s\bullet G}$ should be directly reserved in the low-order model. In summary, the reserved dynamics include the $x_{s\bullet G}$, $x_{f\bullet D}$ and x_{CD}.

The identification method of coupling dynamics is shown in Fig. 10. Under the non-classical SP system, it needs to identify which coupling dynamics get the characteristics of fast or slow dynamics. The identification method is divided into two steps. The first is to figure out the coupling dynamics that behave as slow dynamics. Although the $x_{CD\bullet s}$ originally needed to be reserved as the slow dynamics, identifying them is helpful for the coupling time-scale analysis of system modes. Firstly, fixing the selected global slow dynamics as constant value and establishing the fast subsystem. And the fast eigenvalues will not coincide with the original full-order model if any coupling dynamics are included in selected $x_{s\bullet G}$. Then choose the dynamics of small PF as $x_{CD\bullet s}$, remove it and repeat the fast subsystem establishment until the fast modes coincide. So far, the $x_{CD\bullet s}$ hidden in x_s can be confirmed.

Secondly, focus on the dominant modes and identify the coupling dynamics that behave as fast dynamics. Based on the fast dynamics identified before, $x_{s\bullet G}$ and $x_{CD\bullet s}$ are reserved for model reduction and the accuracy of the reduced-order dominant modes can be determined. Choosing the large PF of x_f as $x_{CD\bullet f}$ and reserve them into the dominant modes again until the dominant modes coincide. In the end, the coupling dynamics can be confirmed, including $x_{CD\bullet f}$ and $x_{CD\bullet s}$.

In conclusion, the method can identify the system coupling dynamics with both fast and slow dynamic components without calculating the numbers of dynamics as well as trial-and-error searching. Therefore, the model reduction can be implemented quickly and accurately.

E. Model Reduction Method for Characterizing Multi-Timescale and Guaranteeing Computational Efficiency

To sum up, the generalized model reduction method of non-classical singular perturbation system can be given in Fig. 11. Firstly, the multi-timescale should be identified by the PF analysis of the dominant modes. Then the slow dynamics and the global fast dynamics can be figured out by the analysis. Secondly, the network can be simplified by equivalent techniques and the system boundary layer can be constructed by the dual time-scale method. The construction of the boundary layer system in (11) and (12) can realize the linear preservation of the system's fast dynamics. Then the fast dynamics are eliminated by the classical SP method in (13). Therefore, the first step of reduction can be confirmed.

Thirdly, after determining the non-classical singular perturbation characteristics, the identification method in Fig. 10 can be carried out. Then it can be considered to re-add the identified coupling dynamics to the first step reduced-order model. Finally, the final reduced-order model that characterizes multi-timescale and guarantees computational efficiency can be obtained under the proposed generalized reduction method.

IV. Model Reduction of Microgrid Clusters Based on Non-Classical Singular Perturbation

A. Equivalent Network Simplification

Based on the analysis in Section II-C, some fast modes are mainly strongly associated with the states of currents of feeders, tie-lines and loads. Besides, before conducting the reduction study, the equivalence of the electrical network is first performed in order to reduce the number of nodes and simplify the system [17], [25]. In this study, the network of feeders can be simplified and combined with the inductance L_f of the *LCL* according to the Kirchhoff's current law under *dq* axis:

$$\Delta i_{oDQi} = \Delta i_{lineDQi} \tag{14}$$

Then, the equivalence of feeders can be given as:

$$\begin{cases} L_f^e = L_f + L_{line} \\ R_f^e = R_f + R_{line} \end{cases} \tag{15}$$

In (14)-(15), $\Delta i_{lineDQi}$ are the currents of the feeders in *dq* axis. L_f and R_f are the output filter inductance and resistance. L_{line} and R_{line} are the feeder inductance and resistance. L_f^e and R_f^e are the output filter inductance and resistance after equivalence.

In addition, the equivalence will lose some modes generated by the network, which are not the focus of this study because of the high-frequency and high-damping characteristics. It should be noted that, although the tie-lines belong to the network and associated with the fast modes, they are the important element of the power flow between MGs. So, the state variables of tie-lines can be regarded as the dominant dynamics of the fast subsystem, which are the non-negligible part of the modeling framework and reserved in the reduced-order model.

This article has been accepted for publication in a future issue of this journal, but has not been fully edited. Content may change prior to final publication. Citation information: DOI10.1109/tsg.2023.3297451

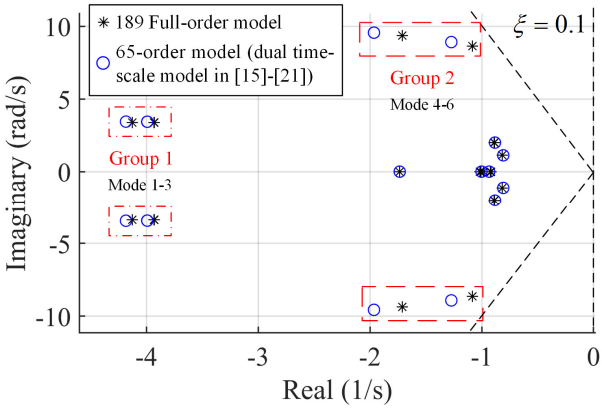

Fig. 12. Comparison between dominant modes of the full-order model and 65-order model.

B. System Boundary Layer Construction and Reduction

1) Reduction of the Load Model

Firstly, the load model can be represented in SP form:

$$-\frac{L_{load}}{R_{load}}\Delta\dot{i}_{loadDQ} = A_{load}\Delta i_{loadDQ} + B_{load1}\Delta\omega_{com} + B_{load2}\Delta v_{pccDQ} \tag{16}$$

Note that the matrices A_{load} and B_{load1} can be obtained the same in [31]. Besides, B_{load2} is related to the load node:

$$B_{load2} = \begin{bmatrix} B_{load2\cdot1} & 0 & 0 \\ 0 & B_{load2\cdot2} & 0 \\ 0 & 0 & B_{load2\cdot3} \end{bmatrix} \text{ while } B_{load2\cdot i} = \begin{bmatrix} -\frac{1}{R_{load\cdot i}} & 0 \\ 0 & -\frac{1}{R_{load\cdot i}} \end{bmatrix}$$

and $\Delta v_{pccDQ} = [\Delta v_{pcc1D}\ \Delta v_{pcc1Q}\ \cdots\ \Delta v_{pcc3D}\ \Delta v_{pcc3Q}]^T$. $L_{load\cdot i}$ is the inductance of load i, and Δv_{pccDQ} is the voltage of PCC in dq axis.

To obtain the boundary layer composed of the load model, the SP parameter ε_{load} can be regarded as $-L_{load}/R_{load}$ then the solution of Δi_{loadDQ} can be obtained by solving the linear equation by gaussian elimination. Finally, the boundary layer composed of loads can be substituted back into the original system for order reduction.

2) Reduction of PV/BESS Units

The PV and BESS units share the same structure of boundary layer because they have the same fast dynamics. The boundary layers of the PV units are established for reduction, and the BESS units are similar. Conducting the appropriate selection of matrix ε, the SP equation of power loop, voltage and current loop, *LCL* filter can be simultaneously combined as follows:

$$\varepsilon_{PV}\dot{\Delta x}_{BL}^{PV} = A_{BL}^{PV}\Delta x_{BL}^{PV} + B_{BL1}^{PV}\Delta i_{oDQ} + B_{BL2}^{PV}\Delta P \tag{17}$$

$$\Delta x_{BL}^{PV} = [\Delta Q_{PV}\ \ \Delta\gamma_{vdq}\ \ \Delta\gamma_{idq}\ \ \Delta i_{ldq}\ \ \Delta v_{odq}]^T \tag{18}$$

The matrices A_{BL}^{PV} and B_{BL}^{PV} can be derived from the ODEs representing the corresponding controllers or components of the boundary layer states Δx_{BL}^{PV}. Then, the solution of fast dynamic can be obtained by solving the linear equation. With the boundary layer substituted into the original system, the remaining dynamics of the PV unit are:

$$[\Delta\delta_{PV}\ \ \Delta P_{PV}\ \ \Delta\alpha_{dc}\ \ \Delta v_{dc}\ \ \Delta i_{odq}]^T \tag{19}$$

Similarly, the remaining dynamics of the BESS unit are:

$$[\Delta\delta_{BESS}\ \ \Delta P_{BESS}\ \ \Delta i_{odq}]^T \tag{20}$$

3) Reduction of DFIG Units

Based on the above analysis, it is able to establish the boundary layer composed of the DFIGs:

$$\varepsilon_{DFIG}\dot{\Delta x}_{BL}^{DFIG} = A_{BL}^{DFIG}\Delta x_{BL}^{DFIG} + B_{BL1}^{DFIG}\Delta x_{SM} + B_{BL2}^{DFIG}\Delta i_{oDQ} + B_{BL3}^{DFIG}\Delta\varphi_{vdq} + B_{BL4}^{DFIG}\Delta P \tag{21}$$

$$\Delta x_{BL}^{DFIG} = [\Delta Q_{DFIG}\ \ \Delta\varphi_{idq}\ \ \Delta\varphi_{dc}\ \ \Delta\eta_{idq}\ \ \Delta u_{dc}\ \ \Delta i_{sdq}\ \ \Delta i_{rdq}\ \ \Delta i_{ldq}\ \ \Delta v_{odq}]^T \tag{22}$$

It is worth noting that this study focuses on complex-conjugate eigenvalues manifesting as damped oscillations (transient performance) while negative real eigenvalues may affect the speed of the system reaching to steady-state (dynamic performance) after being perturbed [36]. Although the state variables η_{idq} are only strongly associated with the two ED modes, they have little contribution to Mode 1-9. Besides, the ED modes have been truncated into two modes in the previous analysis. If the truncated modes can be reproduced in the reduced-order model, the dynamic performance of the original system can be reflected. Therefore, these states are out of consideration in model reduction and can be treated as fast dynamics using the SP method. The matrices A_{BL}^{DFIG} and B_{BL}^{DFIG} can be derived from the ODEs representing the corresponding controllers or components of the boundary layer states Δx_{BL}^{DFIG}. Then, solving the linear equation and obtaining the solution, the remaining dynamics of the DFIG unit are:

$$[\Delta\delta_{DFIG}\ \ \Delta P_{DFIG}\ \ \Delta\alpha_{\omega r}\ \ \underbrace{\Delta\omega_{wheel}\ \ \Delta T_m\ \ \Delta\omega_r}_{\Delta x_{SM}}\ \ \Delta\varphi_{vdq}\ \ \Delta i_{odq}]^T \tag{23}$$

4) Reduced-Order Model under Dual Time-Scale System

After fully obtaining the boundary layer of the MGC system, the SP method in dual time-scale can be applied for order reduction. Applying the network simplification and the boundary layer substituted into the original system, we can obtain the 65-order reduced model by Equation (24):

$$\dot{x}_{MGC\cdot65} = A_{MGC\cdot65}x_{MGC\cdot65} \tag{24}$$

Fig. 12 shows the comparison between the dominant modes of the full-order model and the 65-order model using the dual time-scale reduction model in [15]-[21]. Only the slow dynamics are reserved in this model without identifying the coupling dynamics, Group 1-2 have matching errors as seen in Fig. 12. The errors are reflected in the damping of each mode while the oscillation frequency basically coincides. The damping of the low-order model has become stronger, which cannot accurately reflect the transient performance of the original system. However, after reducing the dynamics by 66%, the 65-order model can also basically restore the dominant oscillation modes of the original system.

C. Coupling Dynamics Identification of Microgrid Clusters

In Section III-D, the identification method of coupling dynamics is proposed and it is applied for the studied MGC system in this part. The first is to separate the coupling dynamics from slow dynamics though they have been already

This article has been accepted for publication in a future issue of this journal, but has not been fully edited. Content may change prior to final publication. Citation information: DOI10.1109/tsg.2023.3297451

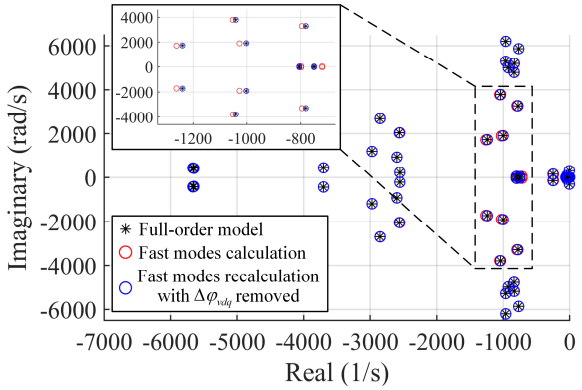

Fig. 13. Comparison between fast eigenvalues of full-order model and the two fast subsystem models.

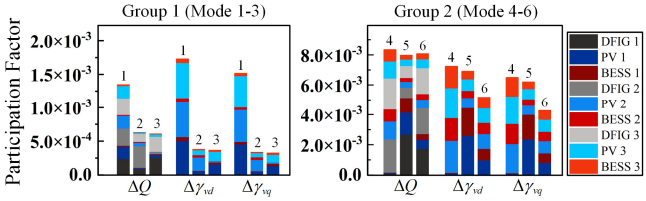

Fig. 14. Participation factor results of some reduced states of Mode 1-6.

reserved in the 65-order model. The selected global slow dynamics $x_{s\text{-}G}$ include all the slow dynamics reserved in Equation (24). According to the flowchart in Fig. 10, fixing them as constant values, it is able to establish the fast subsystem and calculate the remaining fast modes, as shown in Fig. 13. However, some fast modes marked by the dashed boundary have significant errors and the conclusion is negative for coincidence with the full-order model.

In addition, in multi-timescale analysis, it can be found that the coupling time-scale characteristics of Group 1-2 are the most obvious. The participation factor analysis of Group 1-2 carried out in Section II-C illustrates the shaft model Δx_{SM} as well as the voltage loop $\Delta\varphi_{vdq}$ of RSC have slightly less contribution to the dominant modes than the other strongly associated states. However, Δx_{SM} are tended to be preserved as they are the slower mechanical components. Therefore, it is reasonable to choose $\Delta\varphi_{vdq}$ as the coupling dynamics $x_{CD\text{-}s}$. The fast eigenvalues can be recalculated, as also shown in Fig. 13, indicating that the error has been eliminated and all the fast eigenvalues coincide with the original model. Only if the coupling dynamics are correctly selected, the fast eigenvalues can be consistent with the original model. It can be concluded that the state variables $\Delta\varphi_{vdq}$ are the coupling dynamics behaving as slow dynamics.

Secondly, it needs to separate the coupling dynamics from fast dynamics. When $x_{s\text{-}G}$ and $x_{CD\text{-}s}$ are reserved, the 65-order model can be obtained as shown in Fig. 12, which shows that Group 1-2 cannot accurately locate and lose transient performance accuracy in this model. It is necessary to conduct the PF analysis among the dynamics being reduced in the 65-order model and the states of Group 1-2 with large PF are shown in Fig. 14. It should be noted that the PF of the selected state

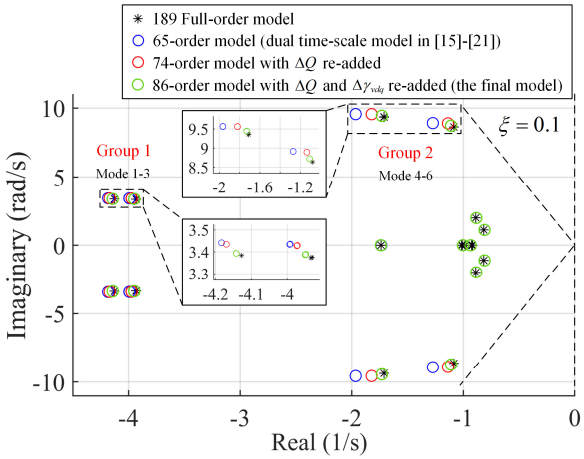

Fig. 15. Comparison between dominant modes of the full-order model, 65-order model, 74-order model and 86-order model.

variables ΔQ and $\Delta\gamma_{vdq}$ is much lower than the other variables that have been reduced in the 65-order model. It is reasonable to speculate that the variables $\Delta\gamma_{vdq}$ have the coupling time-scale characteristics compared with $\Delta\varphi_{vdq}$ under the above analysis. The selected coupling dynamics ΔQ and $\Delta\gamma_{vdq}$ will be re-added to the 65-order model in the following work to verify the accuracy of the identification.

D. Reduced-Order Model of Microgrid Clusters

Based on the 65-order model in (24), the coupling dynamics behaving as fast dynamics should be re-added while the coupling dynamics that behaving as slow dynamics are already reserved in the model. Firstly, the variables ΔQ are added back into the reduced-order model as shown in Fig. 15 (74-order model) which illustrates the improved accuracy of the eigenvalues' location of Group 1-2. Secondly, the re-adding of the PV and BESS voltage loop variables $\Delta\gamma_{vdq}$ is also conducted in Fig. 15. The accuracy of the reduced-order model further improves, especially in Group 1-2 that have the coupling time-scale characteristics. In addition, the proposed model can accurately identify the interactions among different MGs in the clusters. In Modes 1, 6, and 9, the participation of the three MGs is almost the same, as shown in Fig. 8. It can be concluded that the interactions occur in three MGs in these modes. Moreover, Mode 3 is mainly associated with MG 1 and 3, while Mode 4 and 7 are mainly associated with MG 2 and 3. Therefore, there is a wide range of interactions between the MGs in the dominant modes, especially the Group 1-2 that have the coupling time-scale characteristics. Most importantly, the interactions can be investigated after reduction, especially the increased accuracy of coupling time-scale Group 1-2 after re-adding the coupling dynamics. It is noted that if the accuracy of the dominant modes of the reduced-order model can be guaranteed, the MGs interactions exhibited in the modes are also preserved in the proposed reduced-order model.

Therefore, the re-adding can accurately restore the transient performance of the original system. The coupling dynamics are correctly identified for describing the coupling time-scale

This article has been accepted for publication in a future issue of this journal, but has not been fully edited. Content may change prior to final publication. Citation information: DOI10.1109/tsg.2023.3297451

TABLE IV
THE COMPUTATION TIME COMPARISONS OF THE EIGENVALUES OF THE FULL-ORDER, 65-ORDER AND 86-ORDER MODELS

Model	Accuracy	Time	Average time	Time reduction percentage
Full-order model	Original benchmark	85.11s	85.25s	Original benchmark
		85.04s		
		85.61s		
65-order model (The traditional model in [15]-[21])	Lose accuracy	23.36s	23.56s	72.36%
		23.45s		
		23.70s		
86-order model (The proposed model)	High accuracy	27.36s	27.69s	67.52%
		28.00s		
		27.72s		

characteristics of the model, which can obtain the 86-order reduced model with coupling dynamics:

$$\dot{x}_{MGC\cdot 86} = \begin{bmatrix} \dot{x}_{MGC\cdot 65} \\ \dot{x}_{CD\cdot f} \end{bmatrix} = A_{MGC\cdot 86} \begin{bmatrix} x_{MGC\cdot 65} \\ x_{CD\cdot f} \end{bmatrix} \tag{25}$$

The reduced-order model in (25) can reduce the dynamics by 54% and accurately restore the dominant oscillation modes of the original system. Besides, the ED modes can also be accurately truncated into two modes, reflecting the model reduction accuracy. In summary, the 86-order model can not only accurately describe the multi-timescale characteristics but also reduce the computational burden because of the lower-order model. However, in order to more specifically demonstrate the improved computational efficiency in stability analysis of the proposed reduced-order model, further works need to be discussed.

E. Discussions on Efficiency and Applicability of the Reduced-Order Model Stability Computation

Actually, the full-order model is absolutely the most accurate in stability and dynamic characteristic analysis. However, it is complicated to accurately establish the full-order model of the large-scale MGC system. Besides, it suffers from the burden of numerical calculation of stability analysis as well as the burden of small-step or long-time simulation.

On the other hand, the proposed reduced-order model of MGC can guarantee the accuracy of the dominant modes after re-adding the coupling dynamics. Moreover, Table IV shows the computation time comparisons of the eigenvalues of the full-order, 65-order and 86-order models. Noted that all the computations use Intel i7-10700 CPU and 32G RAM under MATLAB R2020b of Windows 11 environment and the results take the average of the three times computation.

It can be seen that the full-order model takes a lot of time to calculate the eigenvalues, which is more than three times as much as the final proposed 86-order model. Besides, the time of 65-order model is slightly shorter than the final model, which is about 28% of the full-order model computation time. However, the 65-order model by the dual time-scale method loses accuracy and it will be out of consideration though it is a bit faster. Furthermore, the final 86-order model reduces the time by more than 67% and only needs one-third of the original model.

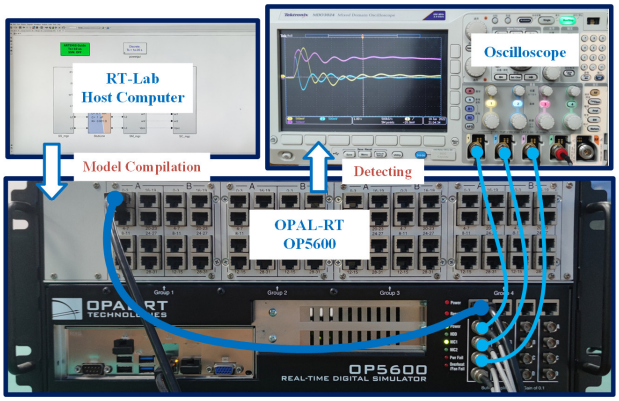

Fig. 16. Real-time simulation environment.

In summary, the proposed generalized method can be applied for model reduction while retaining the necessary dynamics that dominate the system. The computation and simulation of the system can be more efficient, and the system dynamics can also be accurately characterized as well. Practically, the larger-scale system can be established and carried out the numerical calculation using the proposed reduced-order model based on the fundamental conclusion.

V. REAL-TIME SIMULATION RESULTS

A. Real-Time Simulation Setup

RT-Lab is used to execute the full-order model in real-time simulator OPAL-RT OP5600. As shown in Fig. 16, the full-order model created in MATLAB/Simulink can be compiled in RT-Lab and imported into OP5600. The desired variables can be detected by connecting the oscilloscope to the real-time simulator. In addition, the proposed reduced-order model can be operated in the low-order small-signal model.

B. Verification of Model Response

The simulation verification will compare the transient performance of the full-order model and the proposed reduced-order model under system disturbances. The real-time simulation is chosen instead of the full-order small-signal step response to make the results close to the practical real-life operation; thus, the accuracy and the feasibility of the reduced-order model can be verified.

A step load increase for 1kW in PCC 1 is applied in two models respectively and the comparison of the change of the variables for MG 1 is shown in Fig. 17. As can be seen in Fig. 17 (a), the output power responses of the three units in MG 1 of the reduced-order model have similar performance with the full-order model of real-time simulation under load disturbance, which the magnitude of the steady state are the same. Moreover, for the full-order model and the proposed reduced-order model, the output frequencies of the three units have the same response in Fig. 17 (b). They have the same oscillation frequencies and magnitude of the steady-state. And the reactive power response of the proposed reduced-order model also matches the original model. Besides, the *dq*-axis voltage and current of PCC 1 have good performance in the response.

This article has been accepted for publication in a future issue of this journal, but has not been fully edited. Content may change prior to final publication. Citation information: DOI10.1109/tsg.2023.3297451

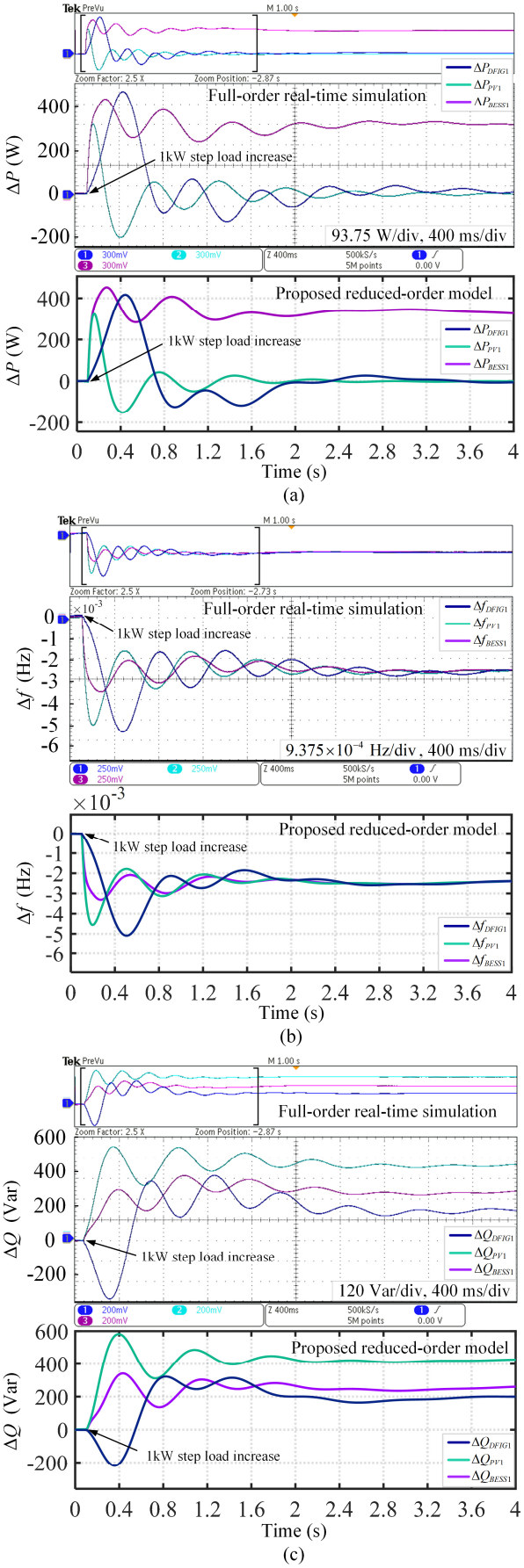

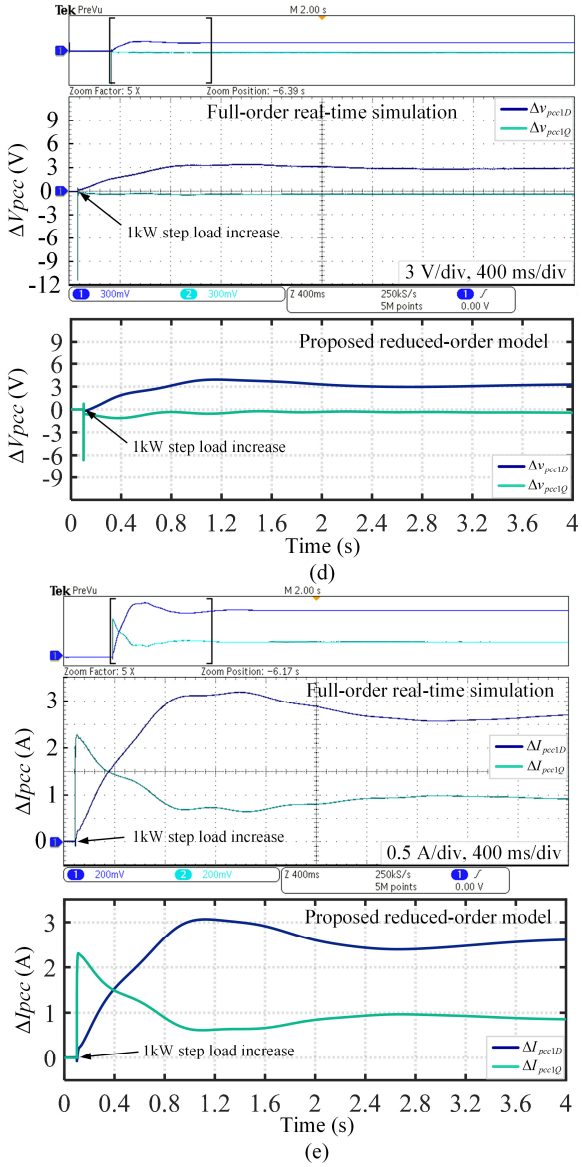

Fig. 17. Comparison of the change of the variables for MG 1 in load step change. (a) Active power. (b) Frequency. (c) Reactive power. (d) *dq*-axis voltage of PCC. (e) *dq*-axis current of PCC.

Under the load transition, the same steady-state value and the similar transition process as the full-order model can be achieved. It should be noted that the oscillations of the small-signal model response curve have a faster decay speed than the real-time simulation, which is also shown in [31], though the model and practical test system have consistent dominant modes in the theoretical analysis. Although slight differences in the response exist in decay speed and overshoot values, the transient performance obtained from the reduced-order model matches with the practical full-order model from real-time simulation. However, the faster decay speed obtained and the differences will not affect the model stability in a large range. In other words, it proves that in numerical simulation, the proposed model has well performance. And compared with the original model, the reduced-order model has similar transient behavior to a certain extent. It can verify the feasibility and

This article has been accepted for publication in a future issue of this journal, but has not been fully edited. Content may change prior to final publication. Citation information: DOI10.1109/tsg.2023.3297451

TABLE V
THE SIMULATION TIME COMPARISONS OF THE POWER AND FREQUENCY RESPONSE OF THE FULL-ORDER AND 86-ORDER MODELS

Model	Power response		Frequency response	
	Time	Average time	Time	Average time
Full-order model	88.18s	88.10s	50.83s	51.22s
	87.35s		51.74s	
	88.76s		51.10s	
86-order model (The proposed model)	45.70s	45.47s	19.75s	19.88s
	45.69s		20.00s	
	45.03s		19.88s	
Time reduction percentage	48.39%		61.19%	

accuracy of the proposed reduced-order model.

C. Verification of Simulation Time

In order to further investigate the computational efficiency of the proposed reduced-order model, it needs to conduct comparisons of the simulation time between the proposed reduced-order model and the original full-order model. Different from the real-time simulation environment, the two small-signal models are established in MATLAB for time verification to observe the response of system variables through the step disturbance as input. The results of the time comparisons of the most concerned power and frequency response are shown in Table V. Both the full-order model and the proposed reduced-order model are implemented in the same MATLAB environment and computer configuration as mentioned above. Besides, the verification tests simulate for one second and the step size is 0.001s.

It can be seen that the proposed 86-order model has significant advantages in computational efficiency, which can reduce the time of the most concerned variables by half or more. The results show the reasonable practical application of the proposed model. Under the premise of ensuring the accuracy of the reduced-order model, it can not only accurately characterize the multi-timescale of the system, but also improve the computational efficiency. In conclusion, the proposed model can play an important role in stability analysis and numerical simulation of the MGC system. Furthermore, the proposed generalized method can also be applied for model reduction as an accurate and efficient analysis tool.

VI. CONCLUSION

The multi-timescale characteristics of multi-source hybrid renewable energy MGC system are analyzed in this paper. It is demonstrated that the electromagnetic and electromechanical transients time-scale of the studied system are interactively coupled; that is, the fast and slow dynamics are not sufficiently separated which presents the non-classical singular perturbation characteristics. In addition, the proposed dynamic classification criterion and the coupling dynamics identification method can effectively separate and identify the coupling dynamics from the fast and slow dynamics. Different from the traditional dual time-scale reduction method, the model reduction introduced in this paper is an effective tool for simplifying the stability analysis of hybrid renewable energy MGC under the non-classical singular perturbation characteristics. It is not simply eliminating the fast dynamics but re-adding the coupling dynamics to restore the accurate dominant modes of the original system. In terms of the stability calculation, with high accuracy, the proposed model reduces the time by 67% compared with the full-order model. Furthermore, on the basis of restoring the dominant modes, the real-time simulations verify the accuracy of the transient performance of the proposed reduced-order model. In terms of the numerical simulation, the proposed model has advantages in computational efficiency. By simulating the most concern variables, it can reduce the time of the power response by 48% and frequency response by 61%. In conclusion, the proposed method and model can not only accurately characterize multi-timescale dynamics of the non-classical singular perturbation system, but also guarantee computational efficiency.

APPENDIX

The matrices A_{SM}, B_{SM1}, B_{SM2} in Equation (1) can be described as (A1)-(A3). H_{wheel}, H_g represent the inertia constants of the wind wheel and AG, respectively; F, k_{tg}, D_{tg} and k_{gear} represent the viscous friction coefficient, mechanical

$$A_{SM}=\begin{bmatrix} -\dfrac{\pi\rho C_p R_{wheel}^{\ 2} v_{wind}^{\ 3}}{4H_{wheel}k_{gear}^{\ 2}\omega_{wheel0}^{\ 2}} & -\dfrac{1}{2H_{wheel}k_{gear}} & 0 \\ k_{tg}k_{gear}-\dfrac{D_{tg}\pi\rho C_p R_{wheel}^{\ 2} v_{wind}^{\ 3}}{4H_{wheel}k_{gear}\omega_{wheel0}^{\ 2}} & -D_{tg}\left(\dfrac{1}{2H_{wheel}}+\dfrac{p}{2H_g}\right) & \dfrac{D_{tg}pF}{2H_g}-k_{tg} \\ 0 & \dfrac{p}{2H_g} & -\dfrac{pF}{2H_g} \end{bmatrix} \quad \text{(A1)}$$

$$B_{SM1}=\begin{bmatrix} 0 & 0 \\ -\dfrac{D_{tg}p^2}{2H_g}L_m i_{rq0} & \dfrac{D_{tg}p^2}{2H_g}L_m i_{rd0} \\ \dfrac{p^2}{2H_g}L_m i_{rq0} & -\dfrac{p^2}{2H_g}L_m i_{rd0} \end{bmatrix} \quad \text{(A2)}$$

$$B_{SM2}=\begin{bmatrix} 0 & 0 \\ \dfrac{D_{tg}p^2}{2H_g}L_m i_{sq0} & -\dfrac{D_{tg}p^2}{2H_g}L_m i_{sd0} \\ -\dfrac{p^2}{2H_g}L_m i_{sq0} & \dfrac{p^2}{2H_g}L_m i_{sd0} \end{bmatrix} \quad \text{(A3)}$$

$$A_{AG}=D\begin{bmatrix} R_sL_r & \omega_0(L_m^{\,2}-L_sL_r)-p\omega_{r0}L_m^{\,2} & -R_rL_m & -p\omega_{r0}L_mL_r \\ -\omega_0(L_m^{\,2}-L_sL_r)+p\omega_{r0}L_m^{\,2} & R_sL_r & p\omega_{r0}L_mL_r & -R_rL_m \\ -R_sL_m & p\omega_{r0}L_mL_s & R_rL_s & \omega_0(L_m^{\,2}-L_sL_r)+p\omega_{r0}L_sL_r \\ -p\omega_{r0}L_mL_s & -R_sL_m & -\omega_0(L_m^{\,2}-L_sL_r)-p\omega_{r0}L_sL_r & R_rL_s \end{bmatrix} \quad \text{(A4)}$$

$$B_{AG1}=D\begin{bmatrix} L_m & 0 \\ 0 & L_m \\ -L_s & 0 \\ 0 & -L_s \end{bmatrix} \quad \text{(A5)} \qquad B_{AG2}=D\begin{bmatrix} L_r & 0 \\ 0 & -L_r \\ -L_m & 0 \\ 0 & L_m \end{bmatrix} \quad \text{(A6)} \qquad B_{AG3}=Dp\begin{bmatrix} -L_m^{\,2}i_{sq0}-L_mL_ri_{rq0} \\ L_m^{\,2}i_{sd0}+L_mL_ri_{rd0} \\ L_sL_mi_{sq0}+L_sL_ri_{rq0} \\ -L_sL_mi_{sd0}-L_sL_ri_{rd0} \end{bmatrix} \quad \text{(A7)}$$

stiffness, damping coefficient and gearbox ratio, respectively; p, ρ, R_{wheel}, C_p and v_{wind} represent the poles of pairs, air density, blade length, performance coefficient of wind wheel and wind speed; ω_{wheel0} is the steady-state value of wind wheel speed.

The matrices $A_{AG}, B_{AG1}, B_{AG2}, B_{AG3}$ in Equation (2) can be described as (A4)-(A7). R_r, L_r, R_s, L_s, L_m represent the rotor resistance and inductance, stator resistance and inductance, mutual inductance, respectively; $D=1/(L_m^{\,2}-L_sL_r)$; $i_{sdq0}, i_{rdq0}, \omega_0, \omega_{r0}$ represent the steady-state value of the stator *dq* currents, rotor *dq* currents, voltage frequency and rotor speed, respectively.

REFERENCES

[1] R. H. Lasseter, "Smart Distribution: Coupled Microgrids," *Proceedings of the IEEE*, vol. 99, no. 6, pp. 1074-1082, June 2011.
[2] Viktor Sebestyén, "Renewable and Sustainable Energy Reviews: Environmental impact networks of renewable energy power plants," *Renewable and Sustainable Energy Reviews*, vol. 151, 111626, Nov. 2021.
[3] R. Wang, Q. Sun, D. Ma and Z. Liu, "The Small-Signal Stability Analysis of the Droop-Controlled Converter in Electromagnetic Timescale," *IEEE Transactions on Sustainable Energy*, vol. 10, no. 3, pp. 1459-1469, July 2019.
[4] M. Rasheduzzaman, J. A. Mueller and J. W. Kimball, "An Accurate Small-Signal Model of Inverter- Dominated Islanded Microgrids Using *dq* Reference Frame," *IEEE Journal of Emerging and Selected Topics in Power Electronics*, vol. 2, no. 4, pp. 1070-1080, Dec. 2014.
[5] Z. Zhao, P. Yang, Y. Wang, Z. Xu and J. M. Guerrero, "Dynamic Characteristics Analysis and Stabilization of PV-Based Multiple Microgrid Clusters," *IEEE Transactions on Smart Grid*, vol. 10, no. 1, pp. 805-818, Jan. 2019.
[6] Y. Peng, Z. Shuai, L. Che, M. Lyu and Z. J. Shen, "Dynamic Stability Improvement and Accurate Power Regulation of Single-Phase Virtual Oscillator Based Microgrids," *IEEE Transactions on Sustainable Energy*, vol. 13, no. 1, pp. 277-289, Jan. 2022.
[7] A. Aderibole, H. H. Zeineldin and M. Al Hosani, "A Critical Assessment of Oscillatory Modes in Multi-Microgrids Comprising of Synchronous and Inverter-Based Distributed Generation," *IEEE Transactions on Smart Grid*, vol. 10, no. 3, pp. 3320-3330, May 2019.
[8] Y. Xu, H. Nian and L. Chen, "Small-Signal Modeling and Analysis of DC-Link Dynamics in Type-IV Wind Turbine System," *IEEE Transactions on Industrial Electronics*, vol. 68, no. 2, pp. 1423-1433, Feb. 2021.
[9] J. K. Kevorkian, J. D. Cole, *Multiple Scale and Singular Perturbation Methods*, Berlin: Springer, 2012.
[10] X. Xu, R. M. Mathur, J. Jiang, G. J. Rogers and P. Kundur, "Modeling of Generators and Their Controls in Power System Simulations Using Singular Perturbations," *IEEE Transactions on Power Systems*, vol. 13, no. 1, pp. 109-114, Feb. 1998.
[11] O. Ajala, A. Domínguez-García, P. Sauer and D. Liberzon, "A Library of Second-Order Models for Synchronous Machines," *IEEE Transactions on Power Systems*, vol. 35, no. 6, pp. 4803-4814, Nov. 2020.
[12] S. Ahmed-Zaid, P. Sauer, M. Pai and M. Sarioglu, "Reduced Order Modeling of Synchronous Machines Using Singular Perturbation," *IEEE Transactions on Circuits and Systems*, vol. 29, no. 11, pp. 782-786, November 1982.
[13] R. K. Varma, R. M. Mathur, G. J. Rogers and P. Kundur, "Modeling Effects of System Frequency Variation in Long-Term Stability Studies," *IEEE Transactions on Power Systems*, vol. 11, no. 2, pp. 827-832, May 1996.
[14] P. Kundur, *Power System Stability and Control*, New York, USA: McGraw-hill, 1994.
[15] M. Rasheduzzaman, J. A. Mueller and J. W. Kimball, "Reduced-Order Small-Signal Model of Microgrid Systems," *IEEE Transactions on Sustainable Energy*, vol. 6, no. 4, pp. 1292-1305, Oct. 2015.
[16] L. Luo and S. V. Dhople, "Spatiotemporal Model Reduction of Inverter-Based Islanded Microgrids," *IEEE Transactions on Energy Conversion*, vol. 29, no. 4, pp. 823-832, Dec. 2014.
[17] I. P. Nikolakakos, H. H. Zeineldin, M. S. El-Moursi and N. D. Hatziargyriou, "Stability Evaluation of Interconnected Multi-Inverter Microgrids Through Critical Clusters," *IEEE Transactions on Power Systems*, vol. 31, no. 4, pp. 3060-3072, July 2016.
[18] I. P. Nikolakakos, H. H. Zeineldin, M. S. El-Moursi and J. L. Kirtley, "Reduced-Order Model for Inter-Inverter Oscillations in Islanded Droop-Controlled Microgrids," *IEEE Transactions on Smart Grid*, vol. 9, no. 5, pp. 4953-4963, Sept. 2018.
[19] M. Kabalan, P. Singh and D. Niebur, "Nonlinear Lyapunov Stability Analysis of Seven Models of a DC/AC Droop Controlled Inverter Connected to an Infinite Bus," *IEEE Transactions on Smart Grid*, vol. 10, no. 1, pp. 772-781, Jan. 2019.
[20] Y. Han et al., "Reduced-Order Model for Dynamic Stability Analysis of Single-Phase Islanded Microgrid With BPF-Based Droop Control Scheme," *IEEE Access*, vol. 7, pp. 157859-157872, 2019.
[21] A. Nayak, M. M. Rayguru, S. Mishra and M. J. Hossain, "A Quantitative Approach for Convergence Analysis of a Singularly Perturbed Inverter-Based Microgrid," *IEEE Transactions on Energy Conversion*, vol. 36, no. 4, pp. 3016-3030, Dec. 2021.
[22] A. Floriduz, M. Tucci, S. Riverso and G. Ferrari-Trecate, "Approximate Kron Reduction Methods for Electrical Networks with Applications to Plug-and-Play Control of AC Islanded Microgrids," *IEEE Transactions on Control Systems Technology*, vol. 27, no. 6, pp. 2403-2416, Nov. 2019.
[23] G. Grdenić, M. Delimar and J. Beerten, "AC Grid Model Order Reduction Based on Interaction Modes Identification in Converter-Based Power Systems," *IEEE Transactions on Power Systems*, vol. 38, no. 3, pp. 2388-2397, May 2023.
[24] V. Purba, B. B. Johnson, M. Rodriguez, S. Jafarpour, F. Bullo and S. V. Dhople, "Reduced-Order Aggregate Model for Parallel-Connected Single-Phase Inverters," *IEEE Transactions on Energy Conversion*, vol. 34, no. 2, pp. 824-837, June 2019.
[25] Z. Shuai, Y. Peng, X. Liu, Z. Li, J. M. Guerrero and Z. J. Shen, "Dynamic Equivalent Modeling for Multi-Microgrid Based on Structure Preservation Method," *IEEE Transactions on Smart Grid*, vol. 10, no. 4, pp. 3929-3942, July 2019.
[26] X. Guo, Z. Lu, B. Wang, X. Sun, L. Wang and J. M. Guerrero, "Dynamic Phasors-Based Modeling and Stability Analysis of Droop-Controlled Inverters for Microgrid Applications," *IEEE Transactions on Smart Grid*, vol. 5, no. 6, pp. 2980-2987, Nov. 2014.
[27] W. Hu, Z. Wu and V. Dinavahi, "Dynamic Analysis and Model Order Reduction of Virtual Synchronous Machine Based Microgrid," *IEEE Access*, vol. 8, pp. 106585-106600, 2020.
[28] Y. Gu, N. Bottrell and T. C. Green, "Reduced-Order Models for Representing Converters in Power System Studies," *IEEE Transactions on Power Electronics*, vol. 33, no. 4, pp. 3644-3654, April 2018.

This article has been accepted for publication in a future issue of this journal, but has not been fully edited. Content may change prior to final publication. Citation information: DOI10.1109/tsg.2023.3297451

[29] Z. Zhao, J. Xie, S. Gong, X. Luo, Y. Wang, C. S. Lai, P. Yang, L. L. Lai and J. M. Guerrero, "Modeling, Oscillation Analysis and Distributed Stabilization Control of Autonomous PV-based Microgrids," *CSEE Journal of Power and Energy Systems*, vol. 9, no. 3, pp. 921-936, May 2023.
[30] Z. Zhao, X. Luo, J. Xie, S. Gong, J. Guo, Q. Ni, C. S. Lai, P. Yang, L. L. Lai and J. M. Guerrero, "Decentralized Grid-Forming Control Strategy and Dynamic Characteristics Analysis of High-Penetration Wind Power Microgrids," *IEEE Transactions on Sustainable Energy*, vol. 13, no. 4, pp. 2211-2225, Oct. 2022.
[31] N. Pogaku, M. Prodanovic and T. C. Green, "Modeling, Analysis and Testing of Autonomous Operation of an Inverter-Based Microgrid," *IEEE Transactions on Power Electronics*, vol. 22, no. 2, pp. 613-625, March 2007.
[32] B. Pal and B. Chaudhuri, *Robust Control in Power Systems*. New York, NY, USA: Springer, 2005.
[33] R. Farmer, "Power Systems Dynamics and Stability," *The Electric Power Engineering Handbook*, L. Grigsby, Ed. Boca Raton, FL, USA: CRC Press, 2001.
[34] V. R. Saksena, J. O'Reilly, and P. V. Kokotovic. "Singular Perturbations and Time-Scale Methods in Control Theory: Survey 1976-1983," *Automatica*, vol. 20, no. 3, pp. 279-293, May 1984.
[35] J. R. Winkelman, J. H. Chow, J. J. Allemong, P. V. Kokotovic. "Multi-Time-Scale Analysis of a Power System," *Automatica*, vol. 16, no. 1, pp. 35-43, Jan. 1980.
[36] A. Aderibole, H. H. Zeineldin and M. Al Hosani, "A Critical Assessment of Oscillatory Modes in Multi-Microgrids Comprising of Synchronous and Inverter-Based Distributed Generation," *IEEE Transactions on Smart Grid*, vol. 10, no. 3, pp. 3320-3330, May 2019.

Zhuoli Zhao (Member, IEEE) received the Ph.D. degree in electrical engineering from South China University of Technology, Guangzhou, China, in 2017. From October 2014 to December 2015, he was a Joint Ph.D. Student and Sponsored Researcher with the Control and Power Research Group, Department of Electrical and Electronic Engineering, Imperial College London, London, U.K. From 2017 to 2018, he was a Research Associate with the Smart Grid Research Laboratory, Electric Power Research Institute, China Southern Power Grid, Guangzhou, China. He is currently an Associate Professor with the School of Automation, Guangdong University of Technology, Guangzhou, China. His research interests include microgrid control and energy management, renewable power generation control and grid-connected operation, modeling, analysis and control of power-electronized power systems and smart grids. He is an Associate Editor of the Protection and Control of Modern Power Systems.

Xi Luo received the M.S. degree in electrical engineering from Guangdong University of Technology, Guangzhou, China, in 2023. He is currently working toward the Ph.D. degree with the Sustainable Energy and Environment Thrust, The Hong Kong University of Science and Technology (Guangzhou), Guangzhou, China. His research interests include microgrid control and operation, control of wind power generation and power electronic converters.

Junhua Wu received the B.E. degree from Guangdong Ocean University Cunjin College, Zhanjiang, China, in 2020. He is currently working toward the master degree in electrical engineering with the School of Automation, Guangdong University of Technology, Guangzhou, China. His research interests include the modeling and stability analysis of microgrids.

Jindian Xie received the B.E. degree from Dongguan University of Technology, Dongguan, China, in 2020, and the M.E. degree in electrical engineering from the School of Automation, Guangdong University of Technology, Guangzhou, China, in 2023. His research interests include the stability analysis and control of microgrid.

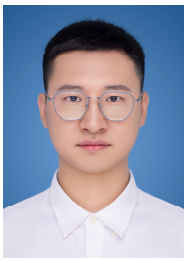

Shaoqing Gong received the B.E. degree from Changchun University of Science and Technology, Changchun, China, in 2020, and the M.S. degree in electrical engineering from the School of Automation, Guangdong University of Technology, Guangzhou, China, in 2023. His research interests include control of microgrid and renewable energy system.

Qiang Ni received the M.Sc. and Ph.D. degrees in electrical engineering from Southwest Jiaotong University, Chengdu, China, in 2013 and 2018, respectively. He is currently a Lecturer with the Guangdong University of Technology, Guangzhou, China. His research interests include forecasting and control technology for multi-energy system, intelligent fault diagnosis and health management of the power electronic system.

Chun Sing Lai (S'11, M'19, SM'20) received the B.Eng. (First Class Hons.) in electrical and electronic engineering from Brunel University London, London, UK, in 2013, and the D.Phil. degree in engineering science from the University of Oxford, Oxford, UK, in 2019.

He is currently a Lecturer with the Department of Electronic and Electrical Engineering and Course Director of MSc Electric Vehicle Systems at Brunel University London. His current research interests are in power system optimization and electric vehicle systems. Dr. Lai was a Technical Program Co-Chair for 2022 IEEE International Smart Cities Conference. He is the Vice-Chair of the IEEE Smart Cities Publications Committee. He is

This article has been accepted for publication in a future issue of this journal, but has not been fully edited. Content may change prior to final publication. Citation information: DOI10.1109/tsg.2023.3297451

an Associate Editor for IEEE Transactions on Systems, Man, and Cybernetics: Systems, IEEE Transactions on Consumer Electronics and IET Energy Conversion and Economics. He is the Working Group Chair for IEEE P2814 and P3166 Standards, an Associate Vice President, Systems Science and Engineering of the IEEE Systems, Man, and Cybernetics Society (IEEE/SMCS) and Co-Chair of the IEEE SMC Intelligent Power and Energy Systems Technical Committee. He is a recipient of the 2022 Meritorious Service Award from the IEEE SMC Society for "meritorious and significant service to IEEE SMC Society technical activities and standards development". He is an IET Member, Chartered Engineer, and Fellow of the Higher Education Academy.

Loi Lei Lai (Life Fellow, IEEE) received the B.Sc. (First Class Hons.), Ph.D., and D.Sc. degrees in electrical and electronic engineering from the University of Aston, Birmingham, UK, and City, University of London, London, UK, in 1980, 1984, and 2005, respectively. Professor Lai is currently a University Distinguished Professor with Guangdong University of Technology, Guangzhou, China. He was a Pao Yue Kong Chair Professor with Zhejiang University, Hangzhou, China, and the Professor and Chair of Electrical Engineering with City, University of London. His current research areas are in smart cities and smart grid. Professor Lai was awarded an IEEE Third Millennium Medal, the IEEE Power and Energy Society (IEEE/PES) UKRI Power Chapter Outstanding Engineer Award in 2000, the IEEE/PES Energy Development and Power Generation Committee Prize Paper in 2006 and 2009, the IEEE Systems, Man, and Cybernetics Society (IEEE/SMCS) Outstanding Contribution Award in 2013 and 2014, the Most Active Technical Committee Award in 2016, and his research team has received a Best Paper Award in the IEEE International Smart Cities Conference in October 2020. Professor Lai is an Associate Editor of the IEEE Transactions on Systems, Man, and Cybernetics: Systems, Editor-in-Chief of the IEEE Smart Cities Newsletter, a member of the IEEE Smart Cities Steering Committee and the Chair of IEEE/SMCS Standards Committee. He was a member of the IEEE Smart Grid Steering Committee; the Director of Research and Development Center, State Grid Energy Research Institute, China; a Vice President for Membership and Student Activities of IEEE/SMCS; and a Fellow Committee Evaluator for the IEEE Industrial Electronics Society. He is a Fellow of IET.